Cellular electron transfer in anaerobic photo-assisted biocathode microbial electrosynthesis systems for acetate production from inorganic carbon (HCO3–)

Cellular electron transfer in anaerobic photo-assisted biocathode microbial electrosynthesis systems for acetate production from inorganic carbon (HCO_3^-)

Liping Huang[a,*], Zijing Xu[a], Yinghong Shi[b], Yu Zhang[a], Gianluca Li Puma[c,*]

[a] Key Laboratory of Industrial Ecology and Environmental Engineering, Ministry of Education (MOE), School of Environmental Science and Technology, Dalian University of Technology, Dalian 116024, China

[b] Weihai Inspection and Research Institute of Products Quality, Standard and Metrology, Weihai 264209, China

[c] Environmental Nanocatalysis & Photoreaction Engineering, Department of Chemical Engineering, Loughborough University, Loughborough LE11 3TU, United Kingdom

Corresponding authors:

lipinghuang@dlut.edu.cn (L. Huang)

g.lipuma@lboro.ac.uk (G. Li-Puma)

The authors declare no competing financial interest.

Abstract

The crucial role played by the cellular electron transfer in the production of acetate

from aqueous inorganic carbon (HCO_3^-, bicarbonate) in anaerobic photo-assisted microbial electrosynthesis (MES) biocathodes incorporating a $WO_3/MoO_3/g\text{-}C_3N_4$ Z-scheme heterojunction and either *Serratia marcescens* Q1 or *Stenotrophomonas* sp. JY6 electrotrophs is disclosed. The electron transfer inhibitor 2,4-dinitrophenol (DNP) diffusing through the bacterial cell membrane was used to alter the ratio of indirect (via H_2) and direct extracellular electron transfer processes, resulting in lower physiological release of extracellular polymeric substances (EPS) and lower acetate production rates under a transitional period. DNP effectively cancelled the synergistic effects on acetate production produced by the photo-irradiation of the $WO_3/MoO_3/g\text{-}C_3N_4$ heterojunction biocathode. The physiological release of EPS with either a compositional diversity (Q1) or varying composition percentages (Q1 or JY6), was correlated to photo-irradiation and to the electrotrophic species, whereas the total amount of EPS was closely related with the electrotrophic DNP-based cellular electron transfer processes. Interestingly, the microorganisms adapted and overcame the impact of DNP after only 4 days of continuous operation and restored their normal physiological metabolism after 7.5 d operation with periodical replenishment of bicarbonate. This study provides a detailed theoretical basis to understand the impact of direct and indirect extracellular electron transfer in hybrid photo-assisted MES biocathodes and elucidates the behavior of non-photosynthetic electrotrophic bacteria favoring high conversion of aqueous inorganic carbon (HCO_3^-) to acetate.

Keywords microbial electrosynthesis; photo-irradiation; cellular electron transfer; electrotroph; acetate production; inorganic carbon reduction

1. Introduction

As an alternative to fossil-fuel-derived commodities, microbial electrosynthesis (MES) has emerged as a sustainable electrochemical process which may be used to drive the microbial metabolism of inorganic carbon (i.e., CO_2 or HCO_3^-) into industrially relevant organic products such as formate, acetate, methanol, butyrate and isopropanol [1-3]. In particular, the biochemical reduction of aqueous inorganic carbon to acetate can be efficiently performed in hybrid photo-assisted MES incorporating anoxic photo(electro)catalytic biocathodes. In such systems, the irradiation of a semiconductor material or heterojunction immobilized over the biocathode produces electron-hole couples. The photo-induced electrons on the conduction band of the semiconductor reduce aqueous protons to H_2, which is further metabolized in-situ by the immobilized electrotrophs with HCO_3^- to produce acetate. Simultaneously, the photo-induced holes are refilled by the electrons arriving from the external circuit. Such mechanism reduces the interfacial resistances creating a supplementary driving force, favoring the non-photosynthetic electrotrophic direct (via e^-) or indirect (vs. H_2) reduction of inorganic carbon [4-6]. In these systems, the photo-irradiation of a semiconductor biocathode immobilized over the cathode further creates a supplementary driving force leading to higher chemicals production in some photo-assisted MES assembled with *Moorella thermoacetica* [7], *Methanosarcina barkeri* [8], *Sporomusa ovata* [6] or *Serratia marcescens* [9-10]. Despite the significant research effort and evident progress made on improving acetate productivity, yield and titers, as well as disclosing the molecular mechanisms of direct

or indirect extracellular electron transfer between microorganisms and electrode, the actual cellular electron transfer mechanism remains enigmatic.

Conventional microbial reduction of inorganic carbon is believed to be associated with cellular electron transfer processes through the cytoplasmic membrane and with the flux of protons through ATP-synthase pumping [11]. Such mechanism has been frequently proven and uncoupled using a cellular metabolic and electron transfer inhibitor such as 2,4-dinitrophenol (DNP). Specifically, DNP can diffuse through the bacterial cell membrane carrying protons to the opposite side of the biomembrane, triggering metabolic changes for metal uptake or hydrogen production in bacteria such as *Cyanobacteria Cyanothece*, *Rhodobacter sphaeroides* or *Bacillus* sp. in the absence of circuital current [11-13]. For example, it has been recently reported that DNP can inhibit the activity of electroactive bacteria such as *Stenotrophomonas* sp. JY6 in bioelectrochemical systems for Cu(II) reduction [14].

The production of hydrogen, as a reducing equivalent and charge mediator to promote the reduction of inorganic carbon to acetate, is strongly dependent on the nature of the electroactive bacteria species in single electrochemical processes [3]. For example, under applied voltages of 0.9 – 1.1 V (versus standard hydrogen electrode, SHE) and under darkness, the non-photosynthetic electrotroph *Stenotrophomonas* sp. JY6 produced H_2 with rates 7.5 times higher than that of the non-photosynthetic electrotroph *Serratia marcescens* Q1 [15-16]. The rate of hydrogen production can be further augmented by the photo-irradiation of semiconductor heterojunctions (e.g., $WO_3/MoO_3/g\text{-}C_3N_4$, $Ag_3PO_4/g\text{-}C_3N_4$, Si/Ti/Ni/Ag, In/P, Ni/Mo or NiS) immobilized

over an anaerobic biocathode [6,8-10]. This in turn triggers higher circuital currents, higher rates of hydrogen production and indirect extracellular electron transfer to *S. marcescens* Q1, yielding higher rates of acetate production through the Wood-Ljungdahl pathway [9-10].

Another important aspect that needs to be elucidated in MES is the adaptive metabolic pathways that a wide group of gram-negative bacteria display as a response and as a protective mechanism to environmental stress [17-18]. The alteration of the environmental conditions around the cells results in the release of extracellular polymeric substances (EPS) composed of varying degrees of saccharides and proteins, however, the role of EPS in cellular electron transfer processes remains controversial [18]. For example, in conventional MES or bioelectrochemical systems, several pure electroactive bacteria are stimulated to secrete EPS, which harbor *c*-type cytochromes assisting extracellular electron transfer, in the presence of a circuital current or both circuital current and heavy metals [15,18-22]. Very recently it has been reported that light exposure affects the structure and function of the bacterial community in photo-assisted anodic bioelectrochemical systems, increasing the storage of polysaccharides over proteins and reducing extracellular electron transfer [23]. However, the physiological release of EPS by different bacteria strains has been scarcely reported particularly in MES incorporating photo-assisted biocathodes. Whether photo-irradiation in such systems plays a key role in the physiological release of EPS, as well as the release of EPS under stressing conditions, remains unanswered. For example, appropriate amounts of DNP stimulate the release of EPS

in conventional aerobic mixed cultures [24], whereas excessive concentrations inhibit the release of EPS in sludge mixed cultures [25].

Under this background, this study mechanistically investigates the cellular electron transfer process of two different non-photosynthetic electrotrophs (*S. marcescens* Q1 and *Stenotrophomonas* sp. JY6) immobilized on photo-assisted MES biocathodes incorporating a $WO_3/MoO_3/g\text{-}C_3N_4$ heterojunction and its impact on acetate production from bicarbonate (HCO_3^-) reduction in water. DNP was used here to alter the cellular electron transfer process within the inner membrane of the electrotrophs and the rates of assimilation of externally generated photo-induced H_2 under anaerobic conditions. This in turn affected the production of acetate and the physiological metabolisms of EPS. Multiple characterization methods were used to evaluate the performance of the photo-assisted MES, the electron transfer process and the rate of release and composition of EPS (exoproteins or exopolysaccharides) including photo-current, scanning electron microscopy equipped with an energy dispersive X-ray spectroscopy (SEM-EDS), cyclic voltammetry (CV), differential pulse voltammetry (DPV), electrochemical impedance spectroscopy (EIS), and three-dimensional excitation-emission matrix (EEM) fluorescence spectroscopy and high-sensitivity flow cytometry. The relationships between cellular electron transfer, photo-irradiation, EPS release, and production of acetate in the photo-assisted biocathode of MES was established. The performance of the MES over long term operation was investigated to establish the condition for recovery of the performance after DNP stress. Overall, this study demonstrates the crucial role played by the

cellular electron transfer in the production of acetate from aqueous inorganic carbon in anaerobic photo-assisted MES biocathodes. Such knowledge should allow greater control of the cellular electron transfer process in photo-assisted MES biocathodes leading to higher rates of conversion of aqueous inorganic carbon (HCO_3^-) to acetate.

2. Materials and methods

2.1. $WO_3/MoO_3/g\text{-}C_3N_4$ synthesis, and photocathode preparation and characterization

The synthesis of $WO_3/MoO_3/g\text{-}C_3N_4$, and the preparation and characterization of the photocathode were as those previously described [9,26]. The $WO_3/MoO_3/g\text{-}C_3N_4$ heterojunction photo-assisted cathode was selected due to favorable biocompatibility, and high conversion of photo-induced electrons for hydrogen evolution. Using this semiconductor heterojunction, the photo-generated holes were efficiently refilled by the circuital electrons produced at the anode, all of which contributed to efficient acetate production from the reduction of inorganic carbon [9].

2.2. Photo-assisted MES reactor, electrotroph inoculation and operation

Each photo-assisted MES reactor comprised an anodic and a cathodic chamber (26 mL operating volume each) separated by a cation exchange membrane (CMI-7000 Membranes International, Glen Rock, NJ) [9]. The anode was a carbon rod (Φ 9 mm × 3 cm, Chijiu Co., Qingdao, China) and the cathode was graphite felt with deposited $WO_3/MoO_3/g\text{-}C_3N_4$ (projected area 4 cm^2; $WO_3/MoO_3/g\text{-}C_3N_4$ loading 1.43 mg/cm^2; ratio of W/Mo oxides and $g\text{-}C_3N_4$ 19.3% (w/w)) [9,26-27]. Prior to each experiment,

all glassware was autoclaved (YX-280A, Shanghai, China) while the electrodes were sterilized on a clean bench (YJ-875B, Shanghai, China) using UV irradiation. All experiments were performed on a sterile anaerobic bench (YQX-II, Xinmiao, Shanghai) to minimize contamination.

The non-photosynthetic electrotrophs *S. marcescens* Q1 (GenBank: MT982676.1) and *Stenotrophomonas* sp. JY6 (GenBank: MT982677.1) capable of metabolizing anaerobically inorganic carbon to acetate in bioelectrochemical systems were initially isolated from well adapted mixed cultures using a progressive dilution method, in an anaerobic glove box (Xinmiao, Shanghai) [9,14,28]. These electrotrophs have been previously applied for the production of acetate from the reduction of inorganic carbon, for the simultaneous production of acetate and removal of Cr(VI) or Cu(II) in pure MESs, or for the same purpose in photo-assisted MESs [9-10,15-16,22,29-30]. These adaptive bacteria are highly tolerant in harsh nutrient barren environments and have been advocated of further investigation [31-34]. After culturing in a sterile medium and incubation for 24 h, the re-suspended electrotroph pellets were individually inoculated in the cathodes of separate MES reactors.

The anaerobic catholyte in each reactor consisted of an aqueous solution of NH_4Cl (2.1 mM), KH_2PO_4 (0.09 mM), vitamins 0.6 mL/L, mineral 0.6 mL/L and $NaHCO_3$ (24 mM). The initial pH (5.8) and the conductivity (103 mS/cm) of the catholyte were adjusted using 10% HCl and 0.6 M KCl, respectively [9-10]. This pH developed efficient bacterial growth and catalytic activity [9-10,16,30].

Oxygen was removed by sparging with ultrapure N_2 for 15 min in an anaerobic

glovebox (YQX-II, Xinmiao, Shanghai). The performance of such photo-assisted MES system is affected by a tradeoff between efficient biocatalysis and light absorption on the bare semiconductor surface of the $WO_3/MoO_3/g\text{-}C_3N_4$: a higher amount of electrotrophs confers superior bioelectrocatalytic activity and stability, whereas a thinner more transparent or patchy electrotrophs layer allow for greater semiconductor photon capture and charges separation [8,35]. Under the same light intensity of 23.3 mW/cm^2 as in this study, by varying the concentration of the electrotrophs in the OD_{600} rang from 0.1 to 0.9, we have previously determined that the highest production of acetate can be achieved with an inoculation of 0.35 in the same photo-assisted MES [9], which was thus further used in these experiments. An appropriate amount (0.25 mM) of DNP (98%, Tianjin Kermel Chemical Industrial Co.) was subsequently added as one-dose to the catholyte. Such concentration was nonfatal on the electroactive bacteria [14] and significantly lower than the half-inhibitory concentration of 2.58 mM to denitrifying bacteria [36]. The reactors were shaken in a table concentrator (30 rpm/min, ZHWY-304, Shanghai, China) under darkness for 12 h prior to exposure to light irradiation. Through this process DNP was biologically removed from the catholyte by diffusion through the bacterial cell membrane [11,36]. The removal of DNP from the catholyte was confirmed by HPLC analysis (Agilent, 1100, equipped with a UV-2300 detector and an Inter Sustain C18 4.6 mm × 250 mm column). The anolyte was made by a 50 mM phosphate buffer, which excluded large change in pH due to hydrolysis and potential effects on cathode performance [9].

The cathode potential in the MES was set to −1.1 V vs. SHE [9-10]. The MES

reactors were operated in fed-batch mode and the cathodes were irradiated by a 100 W iodine tungsten lamp with a light photon flux of 23.3 mW/cm^2 (simulated sunlight) [9,26-27]. Each fed-batch operation lasted 0.5 d and was repeated at least three times.

Experiments with periodical addition of $NaHCO_3$ (up to 7.5 d) were performed to explore the impact of acetate accumulation during a longer operational time. In these experiments, considering the different HCO_3^- metabolic rates of Q1 and JY6 [9,15], 3.0 mL of catholyte was replaced every 36 – 60 h (in the presence of DNP) or 24 – 36 h (in the absence of DNP) with aqueous $NaHCO_3$ solutions at concentrations of 7.3 – 8.0 g/L (Q1) or 6.8 – 7.2 g/L (JY6), to reestablish the initial concentrations of inorganic carbon to 2.0 g/L after each replenishment. All experiments were also performed in triplicates.

Control experiments were performed as follows: The first control was operated in the absence of DNP under photo-irradiation to reflect the impact of DNP on system performance. The second control was conducted under darkness in the presence or in the absence of DNP to explore the influence of photo-irradiation on system performance. The third abiotic control was operated in the absence of electrotroph inoculum with or without DNP under illumination or under darkness to assess the impact exerted by the electrotrophs on system performance.

2.3 Characterization and electrochemical measurement

The photocatalytic properties of the cathode before and after the addition of DNP were assessed by measuring the photocurrent in a 0.1 M Na_2SO_4 solution with a light

illuminance of 26.9 kLux, as previously described [9].

The surface morphology of the photo-assisted biocathodes in the presence or in the absence of DNP at the beginning and at the end of either 0.5 d or 7.5 d operation, was examined by SEM (Nova NanoSEM450, FEI company, USA) equipped with an EDS (X-MAX 20–50 mm^2, Oxford Instruments, UK). Prior to observation, the electrodes were collected and fixed overnight with 2% (v/v) paraformaldehyde and 2% (v/v) glutaraldehyde in 0.1 M cacodylate buffer (pH 7.5, 4 ºC), followed by washing and dehydration in water/ethanol solutions. Samples were then coated with Au/Pt before SEM observation.

CV and EIS were performed with a three-electrode system through a potentiostat (BioLogic, VSP, France) as previously reported [37-38]. The biocathode was the working electrode, assembled with a platinum plate as a counter electrode, a saturated calomel reference electrode and fresh catholyte as electrolyte. Accurate impedance analyses were obtained by fitting the impedance data to an equivalent circuit [39], which modeled the electrochemical reaction occurring at the electrode/electrolyte interface [19-20,22]. The data were fitted through the Zsimpwin software provided by the potentiostat. DPV, which is more sensitive than CV and is normally used to assess the electrochemical activities of the components [17,19-20,22,40], was further used to assess the likely change of outer membrane *c*-type cytochromes of the photo-assisted biocathode in the presence or in the absence of DNP.

The production of hydroxyl radicals in the presence or in the absence of DNP

or/and with photo-irradiation were probed via *p*-hydroxybenzoic acid and HPLC analysis (Agilent, 1100), as previously described [9].

2.4 Analyses and calculations

The concentrations of acetate and residual hydrogen in the headspace of the cathodic chamber were measured using a gas chromatograph (GC7900, Tianmei, China), and the results of acetate (mg/L or mg/L/d) and H_2 ($m^3/m^3/d$) were normalized to the volume of the catholyte and operational time [38,41]. SE-54 cross-linking chromatographic column and a thermal conductivity detector were used for hydrogen quantification using nitrogen as the carrier gas. The temperatures of the column and the injector were both 120 ºC. Acetate was detected using a PEG-20M column and a flame ionization detector using nitrogen as the carrier gas. The temperatures of the column and the injector were both 200 ºC.

The concentration of inorganic carbon was determined according to the standard titration method (DZ/T 0064.49–93) [42]. Biomass on the cathode was quantified as previously described [16].

The electrotrophic viability was assessed by a high-sensitivity flow cytometry (FD FACSCanto flow cytometer, Bioscience) in the presence or in the absence of DNP, with or without illumination, as previously described [9-10].

The amount of EPS released by the cathodic biofilm and its compositional diversity were evaluated at the end of either 0.5 d or 7.5 d operation. Similarly, the amount of EPS and biomass as a function of operational time was determined from a

series of similar anaerobic reactors fed with the same amount of electrotrophs (OD_{600}: 0.35) [9] terminated at 0.5 d, 1.0 d, 1.5 d, 2.0 d, 2.5 d and 3.0 d, respectively. The EPS extraction process was similar to previous description, see Supporting Information (SI) [15,21]. The exopolysaccharides in the EPS was measured by phenol-sulfuric acid method, whereas exoproteins were quantified by the Bradford assay (Bio-Rad, Hercules, CA) using bovine serum albumin as a calibration standard. The EPS composition was characterized by EEM fluorescence spectroscopy (F-7000, Hitachi, Japan) with 1.0 cm quartz cell and a thermostat bath [15,21].

The cathodic charges used for acetate production ($\alpha_{acetate}$), residual H_2 (α_{H2}), electrotrophic growth (α_{growth}), release of exoproteins ($\alpha_{exoproteins}$) and exopolysaccharides ($\alpha_{exopolysaccharides}$) were calculated from Eqs. S1 – 5 [43-45]. The coulombic efficiency for acetate production, residual H_2, bacterial growth, exoproteins and exopolysaccharides was obtained from the ratios of the associated charges and the total coulombs received during the operational period. The mole number of inorganic carbon for acetate production ($\beta_{acetate}$), bacterial growth (β_{growth}), and release of exoproteins ($\beta_{exoproteins}$) and exopolysaccharides ($\beta_{exopolysaccharides}$) (Eqs. S6 – 9), was employed to assess performance of the photo-assisted MES with or without DNP [16,22,43-45].

The relative changes of direct and indirect (via H_2) electron transfers for acetate production were determined by first considering that the amount of H_2 produced in the abiotic photo-assisted MES corresponded to the maximal theoretical production of H_2 in the biotic cathodes, despite this somewhat was an overestimation due to the

presence of the biofilms partially covering the surface of the cathode [46]. This theoretical value was invariable either with or without DNP [9-10]. The difference between this theoretical value and the residual H_2 observed with the biotic cathodes were thus ascribed to the involvement of indirect electron transfer resulting in acetate production (Reactions R1 – R2) [4-5,47]. Thus, the ratio of the hydrogen atoms ascribed to indirect electron transfer from the above calculation and the equivalent hydrogen calculated from the production acetate according to reactions R2 and R3, was thus defined as the percent of indirect (via H_2) electron transfer for acetate production, while the rest was mediated by direct electron transfer (reaction R3).

$$2H^+ + 2e^- \rightarrow H_2 \quad \text{(R1)}$$

$$2HCO_3^- + 4H_2 + H^+ \rightarrow CH_3COO^- + 4H_2O \quad \text{(R2)}$$

$$2HCO_3^- + 9H^+ + 8e^- \rightarrow CH_3COO^- + 4H_2O \quad \text{(R3)}$$

One-way ANOVA in SPSS 19.0 was used to analyze the statistical differences among the data, and all of the data indicated significance levels of $p < 0.05$.

3. Results and discussion

3.1. Negligible impact of •OH to electrotrophs

The potential detrimental impact of •OH radicals on the reproduction and sustainability of the Q1 and JY6 electrotrophs, was assessed by quantitatively probing with *p*-hydroxybenzoic acid and HPLC analysis under a range of experimental conditions (Fig. 1A and B). The peaks at a retention time of 10.3 min observed in the absence or in the presence of DNP, with either Q1 or JY6, corresponded to •OH (0 –

0.70 μM) which is significantly lower than the harmful onset value (3.0 μM) to *Pseudomonas aeruginosa* [48]. In parallel, the amount of inactive Q1 and JY6 electrotrophs observed on the cathodes was 0.6 – 0.7% under normal operation, 0.3 – 0.9% with either DNP and no irradiation or in the absence of DNP but with irradiation, and 0.2 – 0.4% in the controls without propidium iodide staining (Fig. 1C – H and Fig. S1). These results consistent with those in Fig. 1A and B excluded the detrimental effect of •OH radicals on the reproduction and sustainability of the Q1 and JY6 electrotrophs. In addition, the cathodic anaerobic conditions guaranteed the excluding of formation of H_2O_2 and singlet oxygen, and thus avoided their inactivation to the bacteria [9-10]. Negligible changes of photocurrent observed in the presence or in the absence of DNP after 12 h acclimatization in the dark (Fig. 2) further supported the complete diffusion of DNP through the cell membrane of the electrotrophs, as previously reported [11,49] and excluded its photo-degradation.

3.2. MES performance

Both Q1 and JY6 catalyzed $WO_3/MoO_3/g\text{-}C_3N_4$ heterojunction produced significantly higher yields of acetate under photo-irradiation (p = 0.03 (Q1) or 0.00 (JY6)) (Fig. 3A). However, the production of acetate was significantly hampered in the presence of DNP: Q1 (59.5 ± 1.5% decrease, p = 0.01) or JY6 (61.6 ± 0.0% decrease, p = 0.00). This trend also observed under darkness, strongly suggests that cellular electron transfer might regulate the production of acetate in this MES. The decrease in acetate production in the presence of DNP was accompanied with a higher

production rate of residual H_2 (p = 0.01 (Q1) or 0.01 (JY6)) (Fig. 3B), lower circuital current (p = 0.05 (Q1) or 0.02 (JY6)) (Fig. 3C), lower consumption of HCO_3^- (p = 0.00 (Q1) or 0.01 (JY6)) (Fig. 3D), lower coulombic efficiency (p = 0.00 (Q1) or 0.01 (JY6)) (Fig. 3E and F), and lower bacterial growth (p = 0.00 (Q1) or 0.00 (JY6)) (Fig. 3E and G) further confirming the crucial role of DNP in the bacterial cellular electron transfer processes.

The underlying reaction mechanism of the biocathode $WO_3/MoO_3/g\text{-}C_3N_4$ heterojunction comprises the metabolic assimilation of supplementary H_2 produced by photocatalysis with bicarbonate for the biosynthesis of acetate. Thus, a higher rate of residual H_2 under irradiation or under darkness is indicative of a less efficient bioconversion process. The results in Fig. 3 show that DNP has narrowed the positive influential effect of photo-irradiation on acetate production and enlarged the differences for residual H_2 of each electrotroph. The higher rate of residual H_2 observed in the presence of DNP (Fig. 3B) also indicates a change in the distribution of extracellular indirect (via H_2) and direct (via e^-) electron transfer processes. DNP increased the indirect (via H_2) (Q1: 35 ± 2% vs. 22 ± 1%; JY6: 29 ± 0% vs. 18 ±1%) and decreased the direct (Q1: 65 ± 2% vs. 78 ± 1%; JY6: 71 ± 0% vs. 82 ± 1%) extracellular electron transfer processes for the production of acetate (Table 1). These observations provide evidence that cellular electron transfer controls the performance of this photo-assisted MES biocathode immobilizing either Q1 or JY6 electrotrophs.

3.3 SEM observation, and EDS, CV, DPV and EIS analyses

The Q1 (Fig. 4A – D) and JY6 (Fig. 4E – H) electrotrophs were uniformly distributed on the electrodes in the presence (Fig. 4A – B, 4E – F) or in the absence (Fig. 4C – D, 4G – H) of DNP, compared to the abiotic controls (Fig. S2). Although SEM alone cannot be used to exactly quantify biomass growth over the cathode, bacterial growth on the cathode in the presence of DNP decreased, as shown in Fig. 3E and F.

The impact of DNP on the onset reductive potentials was significantly higher than the impact of photo-irradiation (Fig. 4I; Table S1). Whilst a negligible positive shift was observed with photo irradiation (Q1: –0.30 ± 0.01 V vs. –0.32 ± 0.01 V, p = 0.29; JY6: –0.34 ± 0.01 V vs. –0.36 ± 0.01 V , p = 0.29), the presence of DNP resulted in significant negative shift (Q1: –0.39 ± 0.01 V vs. –0.32 ± 0.01 V, p = 0.04; JY6: –0.45 ± 0.01 V vs. –0.36 ± 0.01 V, p = 0.02). Accordingly, DNP halved the reduction peak current (Q1: –0.12 ± 0.02 mA vs. –0.23 ± 0.01 mA, p = 0.04; JY6: –0.10 ± 0.01 mA vs. –0.20 ± 0.01 mA, p = 0.02), whilst photo-irradiation doubled it (Q1: –0.45 ± 0.02 mA vs. –0.23 ± 0.01 mA, p = 0.01; JY6: –0.41 ± 0.02 mA vs. –0.20 ± 0.02 mA, p = 0.02) suggesting a strong increase in overall resistance in the presence of DNP. The shifts observed on the onset reductive potential and reduction peak current with DNP and photo-irradiation were in good agreement with the kinetic results (Fig. 3A – D). The more negative reductive onset potentials imply an increase in the thermodynamic overall free energy of the electron transfer reactions, whereas lower reductive peak currents suggest varying degrees of dynamic mass transfer inhibition [45,50]. Notably, photo-irradiation did not alter the onset reductive potentials observed with DNP (Q1:

–0.39 ± 0.01 V; JY6: –0.45 ± 0.02 V) suggesting that DNP alone was responsible for the change in the thermodynamic overall free energy of the electron transfer reactions. Compared to photo-irradiation alone, the presence of DNP and photo-irradiation led to the same net decrease of the electrodes reduction peak currents for Q1 (–0.23 ± 0.01 mA vs. –0.45 ± 0.02 mA; net: 0.22 ± 0.01 mA) and JY6 (–0.19 ± 0.02 mA vs. –0.41 ± 0.02 mA; net: 0.22 ± 0.01 mA), suggesting an unfavorable impact of DNP to the dynamic mass transfer associated with these two electrotrophs. The abiotic controls always exhibited apparent higher reduction peak potentials and reduction peak currents regardless of the presence of DNP or photo-irradiation (Fig. S3), mainly explained by the bacterial physical attachment to the electrode surface inhibiting the reactive species mass transfer to the electrodes [43,50].

Under darkness, DNP predominantly increased the charge transfer resistance R_{ct} to the electrodes in the EIS (equivalent circuit, Fig. S4) (Q1: 65.5 ± 1.5 Ω vs. 44.0 ± 0.9 Ω, p = 0.01; JY6: 82.6 ± 2.0 Ω vs. 49.1 ± 1.1 Ω, p = 0.00) as observed in conventional bacterial cellular electron transfer [11-13], whereas photo-irradiation appreciably diminished the R_{ct} (Q1: 31.8 ± 0.8 Ω vs. 44.0 ± 0.9 Ω, p = 0.01; JY6: 35.4 ± 0.7 Ω vs. 49.1 ± 1.1 Ω, p = 0.01) (Fig. 4J; Table S1).

DPV analyses showed reduction peak potentials at ~0.026 V in the biotic cathodes while no peaks were observed under abiotic conditions (Fig. 4K). The presence of DNP diminished the reduction peak currents of JY6 more significantly than Q1. The greater reduction peak potential at the typical 0.026 V in the absence of DNP has been confirmed to be indicative of more efficient harboring of outer

membrane *c*-type cytochromes in previous studies. This has been demonstrated for three electrochemically active strains *Shewanella oneidensis* MR1, *Bacillus* sp. WS-XY1 and *Pichia stipites* using multiple techniques including electrochemistry, spectroscopy, atomic force microscopy, and microbiology [19-20]. Accordingly, the higher reduction peak current implies favorable conditions for developing a higher fraction of microbial components for mediating electron transfer processes [19-20]. Considering that we identified a reduction peak potential of ~0.026 V for *Serratia marcescens* Q1 in response to other circumstantial changes (e.g., magnetic field or heavy metals) in MES [22], these results might collectively indicate the likely main components responsible for extracellular electron transfer processes in either Q1 or JY6. EPS analysis further support this interpretation.

3.4 Comparison of EPS, and analysis of fluorescence excitation emission matrix in the presence of either DNP or photo-irradiation

DNP apparently reduced the total release of exoproteins (Fig. 5A, Q1: –29 ± 3%; JY6: –48 ± 4%) and exopolysaccharides (Fig. 5B, Q1: –34 ± 1%; JY6: –44 ± 6%), while photo-irradiation had an insignificant impact (Fig. 5A and B). The unsensitivity to photo-irradiation might be ascribed to the inherent non-photosynthetic characters of these bacteria [9-10,34].

EPS released by Q1 with photo-irradiation and in the presence/absence of DNP contained all five components (Region I: protein (tyrosine)-like matters (E_x/E_m = 200 – 250 nm / 260 – 320 nm); Region II: protein (tryptophan)-like materials (E_x/E_m = 200

– 240 nm / 330 – 370 nm); Region III: polycarboxylate-type humic acid (fulvic acid in ultraviolet region)-like materials (E_x/E_m = 200 – 240 nm / 380–500 nm); Region IV: soluble microbial byproduct-like materials (E_x/E_m = 250 – 450 nm / 260 – 380 nm); and Region V: polycarboxylate-type humic acid (fulvic acid in visible region)-like matters (E_x/E_m = 250 – 450 nm / 380 – 550 nm)) (Fig. 5C and D; Fig. S5), as previously advocated [51-52]. However, component III was not released by Q1 in the absence of photo-irradiation with or without DNP (Fig. 5E and F; Fig. S5), suggesting that fulvic acid-like materials released by Q1 were strongly associated to photo-irradiation. In contrast, JY6 only released components II and IV regardless of the presence of DNP or photo-irradiation (Fig. 5G – J; Fig. S5). Although both electrotrophs released similar amounts of exoproteins and exopolysaccharides (Fig. 5A and B), Q1 exhibited a wider EPS compositional diversity than JY6. Considering also the stronger Q1 reduction peak potential at ~0.026 V, which is typically indicative of harboring of outer membrane *c*-type cytochromes (Fig. 4K) [19-20,22], we are suggesting that the combined effects might had favored extracellular electron transfer processes and therefore an appreciable higher rate of acetate production with Q1 (Fig. 3A). The EPS role as transient media for extracellular electron transfer as also been demonstrated using other electrochemically active bacteria in the absence of DNP [17-20].

Overall, the release of EPS either with a wider compositional diversity (Q1) or with varying component percentages (Q1 or JY6) is primarily closely related to the rate of photo-irradiation, although the fraction of exoproteins and exopolysaccharides

in the EPS were not altered by photo-irradiation. The releases of exoproteins and exopolysaccharides, as well as the peak values of each associated EPS component were always reduced in the presence of DNP. Considering the significant impact of DNP on cellular electron transfer, the electrotrophic physiological release of EPS with compositional diversity and changeable amounts of each component is thus suggested to play a key role in the cellular electron transfer of Q1 or JY6.

3.5 Effect of DNP over a prolonged MES operational time

Over a prolonged operational time up to 3 d, the performance of the biocathode assembled with either Q1 or JY6 under photo-irradiation decreased in the presence of DNP, i.e., lower rates of acetate production (Fig. S6A), higher rates of accumulated residual H_2 (Fig. S6B), lower HCO_3^- consumptions (Fig. S6C), and lower circuital currents (Fig. S6D). Starting from an initial inorganic carbon concentration of 2.0 g/L (as HCO_3^-), the total inorganic carbon utilized for acetate production, bacterial growth and EPS released significantly decreased in the presence of DNP (Fig. 6). The pH insignificantly changed during each fed-batch cycle (with DNP: 6.0 ± 0.1; without DNP: 5.9 ± 0.1) thus, the CO_2/HCO_3^- ratio was unaffected. The cumulative electrons consumed in the presence of DNP and photo-irradiation was lower than that observed in its absence, with or without photo-irradiation (Q1: 1.81 ± 0.01 C vs. 2.53 ± 0.23 C and 2.01 ± 0.19 C, Fig. 6A, B and D; JY6: 1.69 ± 0.02 C vs. 2.36 ± 0.02 C and 1.93 ± 0.03 C, Fig. 6E, F and H). The lowest cumulative cathodic electrons observed for both Q1 and JY6 in the presence of DNP only (Fig. 6C and G) further reflected the

significant negative impact of DNP on the cellular electron transfer process.

3.6 Effect of DNP on MES performance with periodical addition of bicarbonate

The catholyte was periodically supplemented with HCO_3^- to reestablish the original initial concentration of 2.0 g/L, up to a total operational period of 7.5 days with or without DNP, to assess the MES stability over continuous acetate accumulation (Fig. S7). The presence of DNP led to the accumulation of acetate at 7.5 d (Q1: 1157 ± 7 mg/L; JY6: 1017 ± 1 mg/L), almost following linear paths at rates of 154 ± 1 mg/L/d (Q1) and 136 ± 0 mg/L/d (JY6), lower than those in the absence of DNP (Q1: 1721 ± 37 mg/L, 230 ± 5 mg/L/d; JY6: 1450 ± 21 mg/L, 193 ± 3 mg/L/d) (Fig. 7A). Accordingly, the $CE_{acetate}$ was significantly reduced in the presence of DNP.

Interestingly, the alteration of the electrotrophic behavior in the MES in the presence of DNP observed at short operational times was effectively restored after 4 d continuous operation, suggesting a behavioral adaptation of the bacteria. This is shown from the almost constant gradients of acetate accumulation observed after 4 d operation (Fig. 7A) and by the sustained low levels of residual H_2 observed, regardless of the presence DNP (Q1: 0.004 ± 0.000 $m^3/m^3/d$; JY6: 0.025 ± 0.002 $m^3/m^3/d$) (Fig. 7C). Thus the indirect (via H_2) electron transfer processes in the bacteria progressively adapted to the metabolic perturbation induced by DNP after this initial transient period. Further, EIS analyses confirmed the reestablishment of the bacterial performance after an initial inhibition caused by DNP. The dominant and invariable role of the R_{ct} over the R_s and R_{dif} observed at a short operational time was

also confirmed (Table S1). In the presence of DNP and photo-irradiation, the results show an apparent decrease in R_{ct} from 0.5 d to 7.5 d, in contrast to the slight increase in R_{dif} and negligible changes in R_s supporting the bacterial adaptation process.

The cathode morphology and stability observed by SEM were unaffected over a long-term operation of 7.5 d regardless of the presence of DNP, despite the cell aggregates on the electrodes could have been slightly altered during SEM sample preparation. The electrode surfaces were colonized by rod-shaped Q1 (Fig. 7E and G) and JY6 (Fig. 7I and K) with morphologies similar to those observed in the presence (Fig. 7E and I) or in the absence (Fig. 7G and K) of DNP, and those observed at short operational time of 0.5 d (Fig. 4A – H). Further evidence of the cathode stability is provided by the restoration of the initial values of cathodic charges for biomass growth (Eq. S3), which were similar 1.1 ± 0.1 C for Q1 and JY6 after 7.5 d, while much less was observed at a short 0.5 d (Q1: 0.7 ± 0.1 C; JY6: 0.5 ± 0.1 C) (Fig. 3E and F).

Moreover, DNP negligibly affected the rates of W and Mo leaching after 7.5 d operation (Fig. S8), consistent with the EDS results (Table S2). These results excluded the negative effect of electrode degeneration and further confirmed the stability of the WO_3/MoO_3/g-C_3N_4 photocatalytic biocathode which makes significant advances over MES using toxic metals oxides (Cd, Ni or Cs) that dissolve faster after lengthy operation [7-8].

The recovery process of these electrotrophic bacteria was also assessed by EPS analysis. Under photo-irradiation and after 7.5 d operation, Q1 and JY6 released

similar amounts of exoproteins and exopolysaccharides in the presence of DNP, which were very close to those observed without DNP (Fig. 8A and B), and were also negligibly different from those observed without DNP and at 0.5 d (Fig. 5A and B). These results in concert confirmed the electrotrophic recovery from DNP stress through similar physiological release of EPS, in agreement with the results in Fig. 7. The bacteria self-defending mechanism by EPS release is controlled by cellular and environmental signals through a web of complex signaling networks [18]. EPS properties and production rates are known to be influenced by environmental factors such as pH, nutrient supply and redox conditions. High redox potentials, for example, increase the proteins fraction in EPS secreted by *Geobacter sulfurreducens*, presumably attributed to an upregulated expression or excretion of the cytochromes to support a higher electron flux across the EPS matrix. Whereas much higher redox potentials stimulated the production of electrically-nonconductive polysaccharides instead, likely as a protective response to the increased oxidative stress [17-18,53]. Thus, in this study, Q1 and JY6 might have similarly developed effective EPS adaptive regulation processes during this 7.5 d operation, as their self-defending and protecting mechanism from DNP stress.

Surprisingly, component I which was released by Q1 at 0.5 d under photo-irradiation with or without DNP (Fig. 5; Fig. S5), was not detected after 7.5 d (Fig. 8C and D; Fig. S9). Instead, peak values of components IV (961 R.U. vs. 388 R.U.) and V (966 R.U. vs. 333 R.U.) appreciably increased in the presence of DNP (Fig. 8C; Fig. S9), compared to an increase in components II (788 R.U. vs. 540 R.U.)

and V (1029 R.U. vs. 674 R.U.) in the absence of DNP (Fig. 8D; Fig. S9). For JY6, however, the components (II and IV) observed at 0.5 d (Fig. 5; Fig. S5) were confirmed after 7.5 d operation regardless of the presence of DNP (Fig. 8E and F; Fig. S9), but with increased peak values (II: 695 R.U. vs. 296 R.U.; IV: 637 R.U. vs. 305 R.U.). Since the amounts of exoproteins and exopolysaccharides remained unchanged regardless of the presence of DNP at 7.5 d (Fig. 8A and B), conversely to the sharp decreases observed at 0.5 d (Fig. 5A and B), we suggest that the prevailing regulating mechanism of these electrotrophic bacteria to restore their metabolic behavior involves the physiological release of EPS with either compositional diversity (Q1) or variable components amounts (JY6 or Q1).

4. Conclusions

This study has stressed the crucial role played by the cellular electron transfer in the production of acetate from aqueous inorganic carbon in anaerobic photo-assisted MES biocathodes incorporating a $WO_3/MoO_3/g\text{-}C_3N_4$ heterojunction and either *S. marcescens* Q1 or *Stenotrophomonas* sp. JY6 electrotrophs. Introducing an electron transfer inhibitor of DNP within the bacterial cell membranes proved that the cellular electron transfer plays a key role in the performance of these photo-assisted MES systems where DNP altered the ratios of indirect (via H_2) and direct extracellular electron transfer processes, resulting in lower EPS amounts and lower acetate production rates under a transitional period. The physiological release of EPS with either a compositional diversity (Q1) or varying composition percentages (Q1 or JY6),

was correlated to photo-irradiation and to the electrotrophic species, whereas the total amount of EPS was closely related with the rates of cellular electron transfer processes of both electrotrophs. This correlation in photo-assisted MES would thus allow control over the cellular electron transfer process leading to high rates of conversion of aqueous inorganic carbon (HCO_3^-) to acetate.

Interestingly, the microorganisms adapted and overcame the impact of DNP after only 4 days of continuous operation and restored their normal physiological metabolism after 7.5 d operation with periodical replenishment of bicarbonate. This effect was shown to be correlated with the electrotrophic physiological metabolism of EPS release in terms of varying amounts or compositional diversity.

Overall, these results provide a more detailed theoretical basis to investigate the interaction mechanism of photo-irradiation, cellular electron transfer, and electrotrophic physiological EPS metabolism, which is crucial for efficient acetate production from aqueous bicarbonate in photo-assisted MES.

Conflicts of interest

There are no conflicts to declare.

Acknowledgements

The authors gratefully acknowledge financial support from the National Natural Science Foundation of China (Nos. 52070032 and 21777017) and the Fundamental Research Funds for the Central Universities (No. DUT21LAB101).

References

[1] H.R. Jhong, S. Ma, P.J.A. Kenis, Electrochemical conversion of CO_2 to useful chemicals: current status, remaining challenges, and future opportunities, Curr. Opin. Chem. Eng. 2 (2013) 191-199.
[2] Y. Jiang, H.D. May, L. Lu, P. Liang, X. Huang, Z.J. Ren, Carbon dioxide and organic waste valorization by microbial electrosynthesis and electro-fermentation, Water Res. 149 (2019) 42-55.
[3] A. Prévoteau, J.M. Carvajal-Arroyo, R. Ganigué, K. Rabaey, Microbial electrosynthesis from CO_2: forever a promise? Curr. Opin. Biotechnol. 62 (2020) 48-57.
[4] S. Cestellos-Blanco, H. Zhang, J.M. Kim, Y. Shen, P. Yang, Photosynthetic semiconductor biohybrids for solar-driven biocatalysis, Nat. Catal. 3 (2020) 245-255.
[5] P. Lzadi and E. Yu, Realizing full potential of bioelectrochemical and photoelectrochemical systems, Joule 4 (2020) 2085-2087.
[6] Y. Su, S. Cestellos-Blanco, J.M. Kim, Y. Shen, Q. Kong, D. Lu, C. Liu, H. Zhang, Y. Cao, P. Yang, Close-packed nanowire-bacteria hybrids for efficient solar-driven CO_2 fixation, Joule 4 (2020) 800-811.
[7] K.K. Sakimoto, A.B. Wong, P. Yang, Self-photosensitization of nonphotosynthetic bacteria for solar-to-chemical production, Science 351 (2016) 74-77.
[8] E.M. Nichols, J.J. Gallagher, C. Liu, Y. Su, J. Resasco, Y. Yu, Y. Sun, P. Yang, M.C.Y. Chang, C.J. Chang, Hybrid bioinorganic approach to solar-to-chemical conversion, Proc. Natl. Acad. Sci. U. S. A. 37 (2015) 11461-11466.
[9] Z. Cai, L. Huang, X. Quan, Z. Zhao, Y. Shi, G. Li Puma, Acetate production from inorganic carbon (HCO_3^-) in photo-assisted biocathode microbial electrosynthesis systems using $WO_3/MoO_3/g\text{-}C_3N_4$ heterojunctions and *Serratia marcescens* species, Appl. Catal. B-Environ. 267 (2020) 118611.
[10] W. Kong, L. Huang, X. Quan, Z. Zhao, G. Li Puma, Efficient production of acetate from inorganic carbon (HCO_3^-) in microbial electrosynthesis systems incorporating $Ag_3PO_4/g\text{-}C_3N_4$ anaerobic photo-assisted biocathodes, Appl. Catal. B-Environ. 284 (2021) 119696.
[11] N.J. Skizim, G.M. Ananyev, A. Krishnan, G. Charles Dismukes, Metabolic pathways for photobiological hydrogen production by nitrogenase- and hydrogenase-containing unicellular *Cyanobacteria Cyanothece*, J. Biol. Chem. 287 (2012) 2777-2786.
[12] S. Luo, X. Xiao, Q. Xi, Y. Wan, L. Chen, G. Zeng, C. Liu, H. Guo, J. Chen, Enhancement of cadmium bioremediation by endophytic bacterium *Bacillus* sp. L14 using industrially used metabolic inhibitors (DCC or DNP), J. Hazard. Mater. 190 (2011) 1079-1082.
[13] L. Gabrielyan, H. Sargsyan, A. Trchounian, Novel properties of photofermentative biohydrogen production by purple bacteria *Rhodobacter sphaeroides*: effects of protonophores and inhibitors of responsible enzymes, Microb. Cell Fact. 14 (2015) 131.
[14] J. Shen, L. Huang, P. Zhou, X. Quan, G. Li Puma, Correlation between circuital current, Cu(II) reduction and cellular electron transfer in EAB isolated from

Cu(II)-reduced biocathodes of microbial fuel cells, Bioelectrochemistry 114 (2017) 1-7.
[15] J. Hou, L. Huang, P. Zhou, Y. Qian, N. Li, Understanding the interdependence of strain of electrotroph, cathode potential and initial Cu(II) concentration for simultaneous Cu(II) removal and acetate production in microbial electrosynthesis systems, Chemosphere 243 (2020) 125317.
[16] X. Song, L. Huang, H. Lu, P. Zhou, M. Wang, N. Li, An external magnetic field for efficient acetate production from inorganic carbon in *Serratia marcescens* catalyzed cathode of microbial electrosynthesis system, Biochem. Eng. J. 155 (2020) 107467.
[17] G. Yang, L. Huang, Z. Yu, X. Liu, S. Chen, J. Zeng, S. Zhou, L. Zhuang, Anode potentials regulate *Geobacter* biofilms: New insights from the composition and spatial structure of extracellular polymeric substances, Water Res. 159 (2019) 294-301.
[18] H. Yu, Molecular insights into extracellular polymeric substances in activated sludge, Environ. Sci. Technol. 54 (2020) 7742-7750.
[19] Y. Xiao, E. Zhang, J. Zhang, Y. Dai, Z. Yang, H.E.M. Christensen, J. Ulstrup, F. Zhao, Extracellular polymeric substances are transient media for microbial extracellular electron transfer, Sci. Adv. 3 (2017) e1700623.
[20] Y. Xiao and F Zhao, Electrochemical roles of extracellular polymeric substances in biofilms, Curr. Opin. Electrochem. 4 (2017) 206-211.
[21] X. Hou, L. Huang, P. Zhou, F. Tian, Y. Tao, G. Li Puma, Electrosynthesis of acetate from inorganic carbon (HCO_3^-) with simultaneous hydrogen production and Cd(II) removal in multifunctional microbial electrosynthesis systems (MES), J. Hazard. Mater. 371 (2019) 463-473.
[22] S. Sun, L. Huang, X. Song, P. Zhou, An external magnetic field moderating Cr(VI) stress for simultaneous enhanced acetate production and Cr(VI) removal in microbial electrosynthesis system, Environ. Res. 193 (2021) 110550.
[23] M. Sui, Y. Li, Y. Jiang, Y. Zhang, L. Wang, W. Zhang, X. Wang, Light exposure interferes with electroactive biofilm enrichment and reduces extracellular electron transfer efficiency, Water Res. 188 (2021) 116512.
[24] Y. Wang, D. Wei, K. Li, B. Wang, L. Shi, G. Zhang, X. Wang, B. Du, Q. Wei, Response of extracellular polymeric substances to the toxicity of 2,4-dichlorophenol in aerobic granular sludge system: production and interaction mechanism, RSC Adv. 42 (2015) 33016-33022.
[25] A. Ding, D. Lin, Y. Zhao, H.H. Ngo, W. Guo, L. Bai, X. Luo, G. Li, N. Ren, H. Liang, Effect of metabolic uncoupler 2,4-dinitrophenol (DNP) on sludge properties and fouling potential in ultrafiltration membrane process, Sci. Total Environ. 650 (2019) 1882-1888.
[26] Q. Wang, L. Huang, X. Quan, G. Li Puma, Sequential anaerobic and electro-Fenton processes mediated by W and Mo oxides for degradation/mineralization of azo dye methyl orange in photo assisted microbial fuel cells, Appl. Catal. B-Environ. 245 (2019) 672-680.
[27] Q. Wang, Z. Cai, L. Huang, Y. Pan, X. Quan, G. Li Puma, Intensified degradation

and mineralization of antibiotic metronidazole in photo-assisted microbial fuel cells with Mo-W catalytic cathodes under anaerobic or aerobic conditions in the presence of Fe(III), Chem. Eng. J. 376 (2019) 119566.
[28] Y. Tao, H. Xue, L. Huang, P. Zhou, W. Yang, X. Quan, J. Yuan, Fluorescent probe based subcellular distribution of Cu(II) ions in living electrotrophs isolated from Cu(II)-reduced biocathodes of microbial fuel cells, Bioresour. Technol. 225 (2017) 316-325.
[29] X. Hou, L. Huang, P. Zhou, Synergetic interaction of magnetic field and loaded magnetite for enhanced acetate production in biocathode of microbial electrosynthesis system, Int. J. Hydrogen Energ. 46 (2021) 7183-7194.
[30] L. Huang, S. Song, Z. Cai, P. Zhou, G. Li Puma, Efficient conversion of bicarbonate (HCO_3^-) to acetate and simultaneous heavy metal Cr(VI) removal in photo-assisted microbial electrosynthesis systems combining WO_3/MoO_3/g-C_3N_4 heterojunctions and *Serratia marcescens* electrotroph, Chem. Eng. J. 406 (2021) 126786.
[31] L. Huang, L. Gan, N. Wang, X. Quan, B.E. Logan, G. Chen, Mineralization of pentachlorophenol with enhanced degradation and power generation from air cathode microbial fuel cells, Biotechnol. Bioeng. 109 (2012) 2211-2221.
[32] S. Wang, L. Huang, L. Gan, X. Quan, N. Li, G. Chen, L. Lu, D. Xing, F. Yang, Combined effects of enrichment procedure and non-fermentable or fermentable cosubstrate on performance and bacterial community for pentachlorophenol degradation in microbial fuel cells, Bioresour. Technol. 120 (2012) 120-126.
[33] F. Kong, A. Wang, H. Ren, L. Huang, M. Xu, H. Tao, Improved dechlorination and mineralization of 4-chlorophenol in a sequential biocathode-bioanode bioelectrochemical system with mixed photosynthetic bacteria, Bioresour. Technol. 158 (2014) 32-38.
[34] L. Huang, X. Xing, P. Zhou, G. Li Puma, Mixotrophic bacteria for environmental detoxification of contaminated waste and wastewater, Appl. Microbiol. Biotechnol. 105 (2021) 6627-6648.
[35] F. Fischer, Photoelectrode, photovoltaic and photosynthetic microbial fuel cells, Renew. Sust. Energ. Rev. 90 (2018) 16-27.
[36] Z. Zhang, P. Zheng, W. Li, R. Wang, A. Ghulam, Effect of organic toxicants on the activity of denitrifying granule sludge, Environ. Technol. 36 (2015) 699-705.
[37] Y. Tian, L. Huang, X. Zhou, C. Wu, Electroreduction of hexavalent chromium using a polypyrrole-modified electrode under potentiostatic and potentiodynamic conditions, J. Hazard. Mater. 225 (2012) 15-20.
[38] Q. Wang, L. Huang, Y. Pan, P. Zhou, X. Quan, B.E. Logan, H. Chen, Cooperative cathode electrode and in situ deposited copper for subsequent enhanced Cd(II) removal and hydrogen evolution in bioelectrochemical systems, Bioresour. Technol. 200 (2016) 565-571.
[39] Z. He and F. Mansfeld, Exploring the use of electrochemical impedance spectroscopy (EIS) in microbial fuel cell studies, Energy Environ. Sci. 2 (2009) 215-219.
[40] S. Li, G. Sheng, Y. Cheng, H. Yu, Redox properties of extracellular polymeric

substances (EPS) from electroactive bacteria, Sci. Rep. 6 (2016) 39098.
[41] Y. Chen, J. Shen, L. Huang, Y. Pan, X. Quan, Enhanced Cd(II) removal with simultaneous hydrogen production in biocathode microbial electrolysis cells in the presence of acetate or $NaHCO_3$, Int. J. Hydrogen Energ. 41 (2016) 13368-13379.
[42] American Public Health Association, American Water Works Association, Water Pollution Control Federation. Standard methods for the examination of water and wastewater. 20th edn. American Public Health Association, Washington, DC. 1998.
[43] L. Huang, Y. Liu, L. Yu, X. Quan, G. Chen, A new clean approach for production of cobalt dihydroxide from aqueous Co(II) using oxygen-reducing biocathode microbial fuel cells, J. Clean. Prod. 86 (2015) 441-446.
[44] L. Huang, F. Tian, Y. Pan, L. Shan, Y. Shi, B.E. Logan, Mutual benefits of acetate and mixed Tungsten and Molybdenum for their efficient removal in 40 L microbial electrolysis cells, Water Res. 162 (2019) 358-368.
[45] F. Ameen, W.A. Alshehri, S. Al Nadhari, Effect of electroactive biofilm formation on acetic acid production in anaerobic sludge driven microbial electrosynthesis, ACS Sustain. Chem. Eng. 8 (2020) 311-318.
[46] M. Sharma, S. Bajracharya, S. Gildemyn, S.A. Patil, Y. Alvarez Gallego, D. Pant, K. Rabaey, X. Dominguez-Benetton, A critical revisit of the key parameters used to describe microbial electrochemical systems, Electrochim. Acta 140 (2014) 191-208.
[47] L. Jourdin and T. Burdyny, Microbial electrosynthesis: Where do we go from here? Trends Biotechnol. 39 (2021) 359-369.
[48] B. Stenuit, L. Eyers, R. Rozenberg, J.L. Habib-Jiwan, S. Matthijs, P. Cornelis, S.N. Agathos, Denitration of 2,4,6-trinitrotoluene in aqueous solutions using small-molecular-weight catalyst(s) secreted by *Pseudomonas aeruginosa* ESA-5, Environ. Sci. Technol. 43 (2009) 2011-2017.
[49] Z. Liang and Z. Hu, Biodegradation of nitrophenol compounds and the membrane fouling trends in different submerged membrane bioreactors, J. Membrane Sci. 415-416 (2012) 93-100.
[50] X. Dominguez-Benetton, S. Sevda, K. Vanbroekhoven, D. Pant, The accurate use of impedance analysis for the study of microbial electrochemical systems, Chem. Soc. Rev. 4 (2012) 7228-7246.
[51] W. Chen, P. Westerhoff, J.A. Leenheer, K. Booksh, Fluorescence excitation-emission matrix regional integration to quantify spectra for dissolved organic matter, Environ. Sci. Technol. 37 (2003) 5701-5710.
[52] F. Kang, P.J. Alvarez, D. Zhu, Microbial extracellular polymeric substances reduces Ag^+ to silver nanoparticles and antagonize bactericidal activity, Environ. Sci. Technol. 48 (2014) 316-322.
[53] D. Liu and W. Li, Potential-dependent extracellular electron transfer pathways of exoelectrogens, Curr. Opin. Chem. Biol. 59 (2020) 140-146.

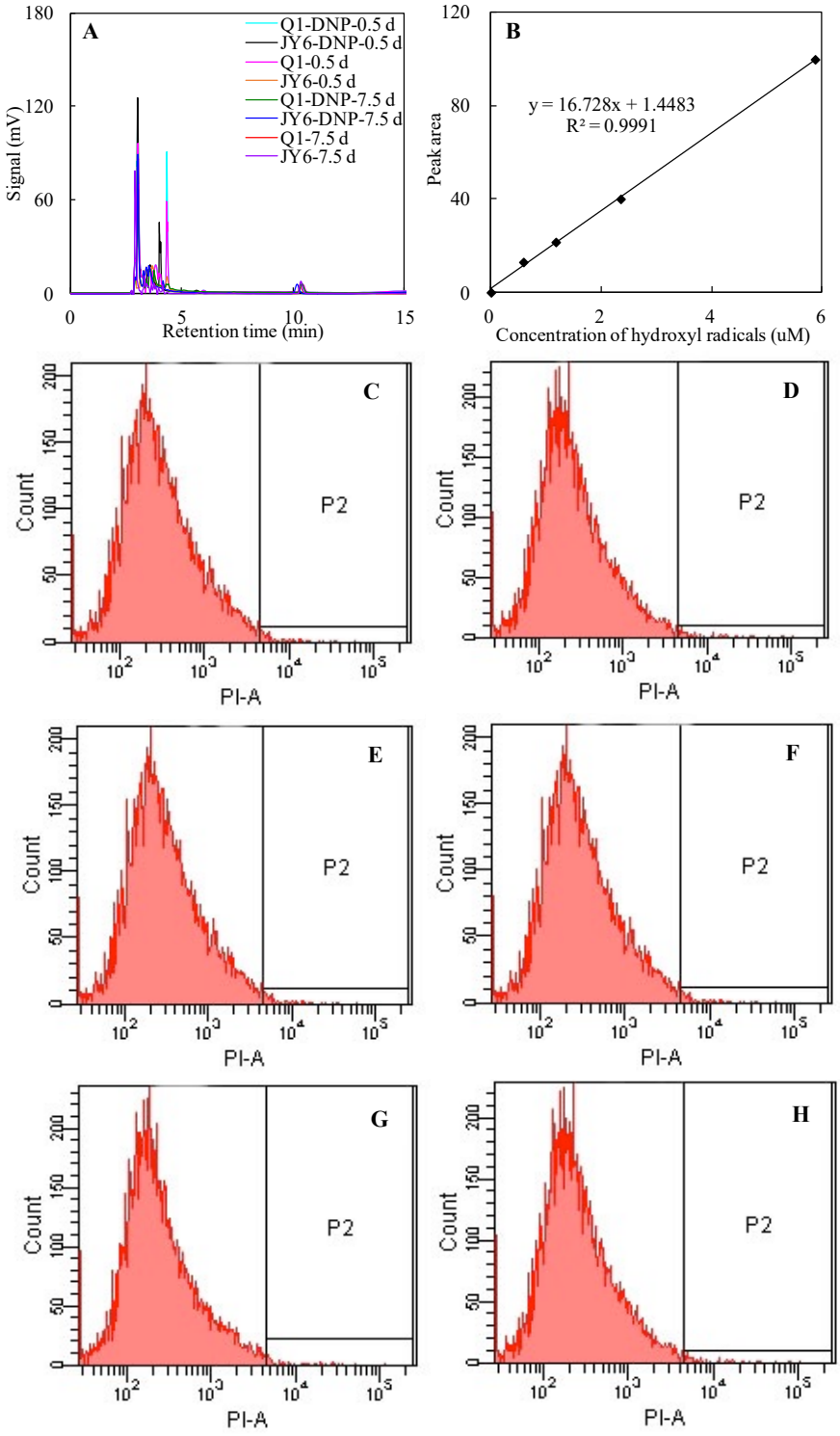

Figure 1 Comparison of absorbance peak of *p*-hydroxybenzoic acid in HPLC as a probe of hydroxyl radicals under various cathode electrodes (A), and the established standard curve (B). Flow cytometry analysis of live/dead *S. marcescens* Q1 (C, D and G) or *Stenotrophomonas* sp. JY6 (E, F and H) on the cathodes of $WO_3/MoO_3/g\text{-}C_3N_4$ in the presence of DNP and light illumination (C and E), or sole light illumination (D and F) or individual DNP (G and H) upon propidium iodide staining.

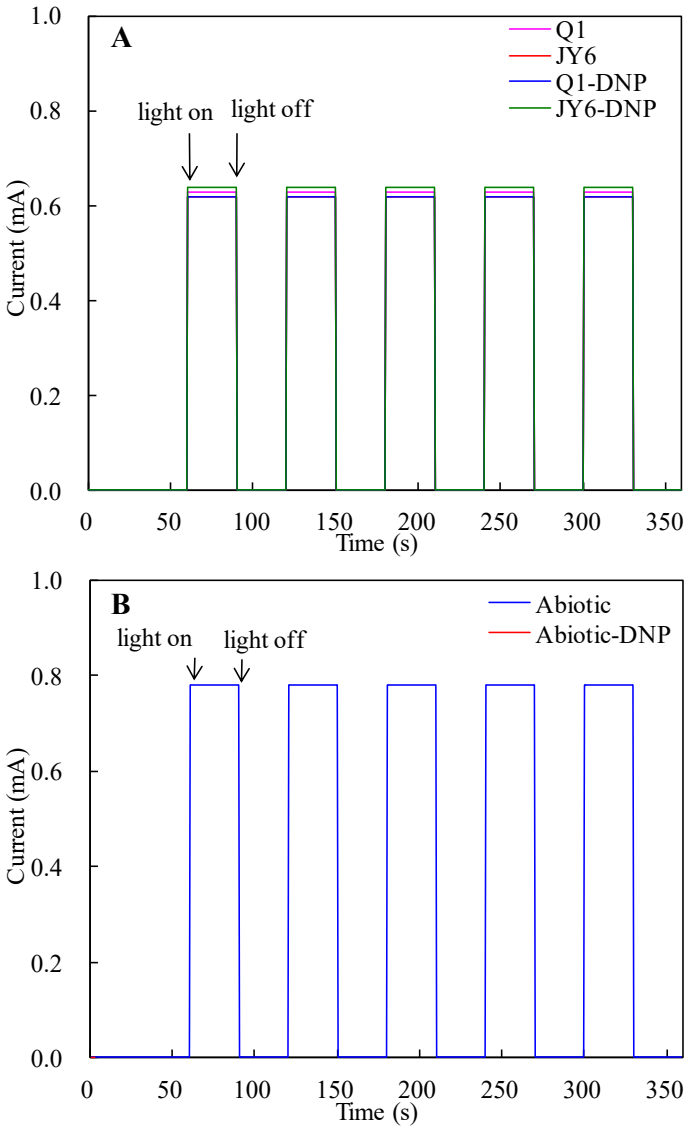

Figure 2 Photocurrent measurements for the WO_3/MoO_3/g-C_3N_4/graphite felt cathodes under the *S. marcescens* Q1, the *Stenotrophomonas* sp. JY6 (A), or the abiotic conditions (B) in 1.0 M Na_2SO_4 aqueous solution in the presence or in the absence of DNP.

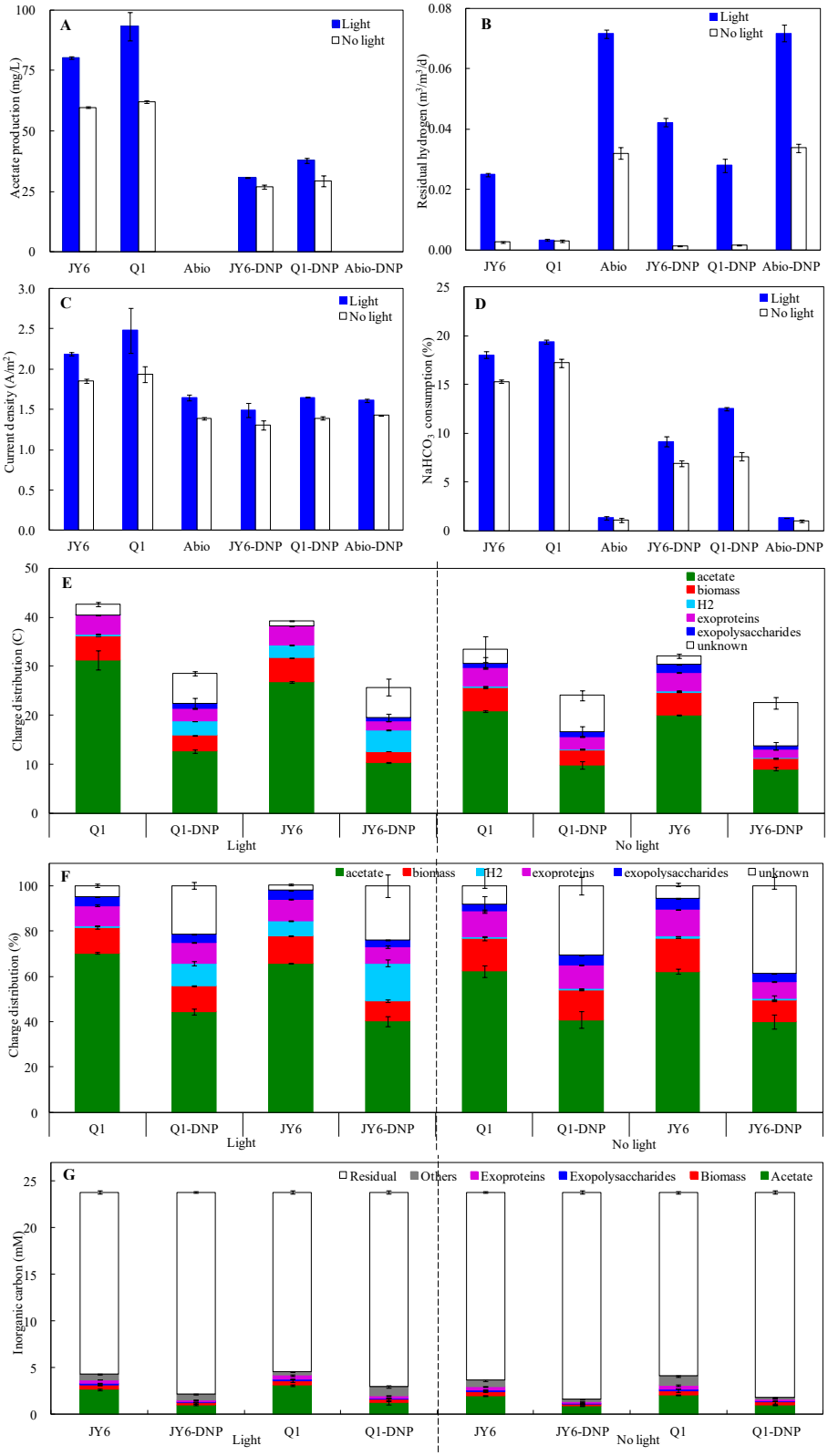

Figure 3 Comparison of acetate production (A), residual hydrogen (B), circuital current (C), consumption of inorganic carbon (D), cathodic charge distribution (E), coulombic efficiency (F), and distribution of total carbon (G) in the cathode of MES incorporated with the *S. marcescens* Q1 or the *Stenotrophomonas* sp. JY6 in the presence or in the absence of DNP or photo-irradiation (operational time: 0.5 d).

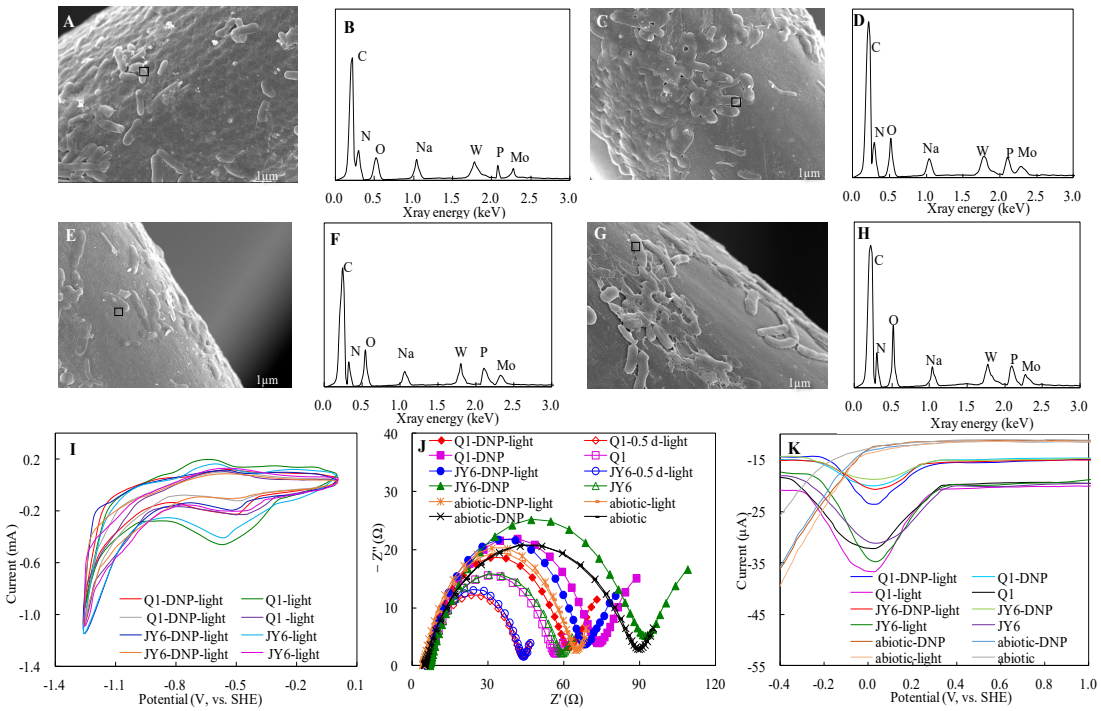

Figure 4 SEM observation (A, C, E and G), EDS spectra (B, D, F and H), CV (I), EIS (J), and differential pulse voltammetry (DPV) (K) of cathodes of the *S. marcescens* Q1 (A – D) or the *Stenotrophomonas* sp. JY6 (E – H) in the presence (A, B, E, F, I – K) or in the absence (C, D, G, H, I – K) of DNP (operational time: 0.5 d).

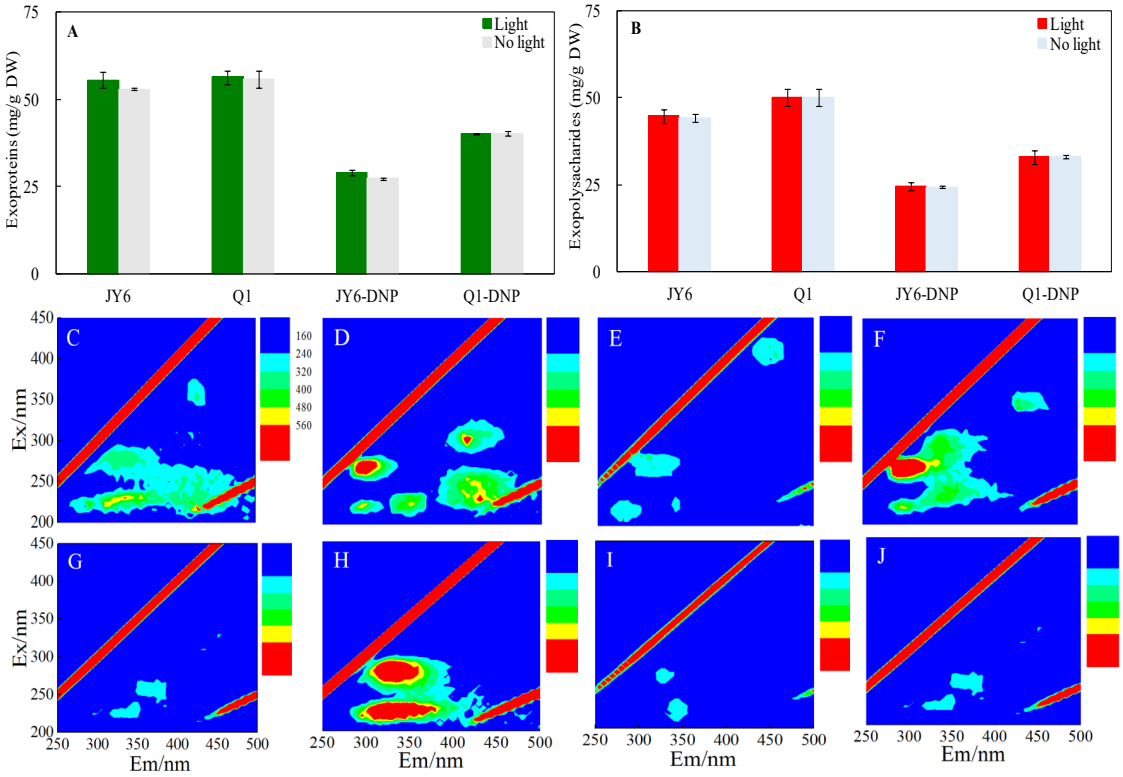

Figure 5 Comparison of exoproteins (A), exopolysaccharides (B), and three-dimensional excitation-emission matrix (EEM) fluorescence spectroscopy of extracellular polymer substances (C – J) produced by either cathodic *S. marcescens* Q1 (A, B, C – F) or *Stenotrophomonas* sp. JY6 (A, B, G – J) biofilms in the presence of either DNP (A – C, E, G and I) or photo-irradiation (A – C, D, G and H), or in the absence of DNP and photo-irradiation (A, B, F and J) (operation time: 0.5 d).

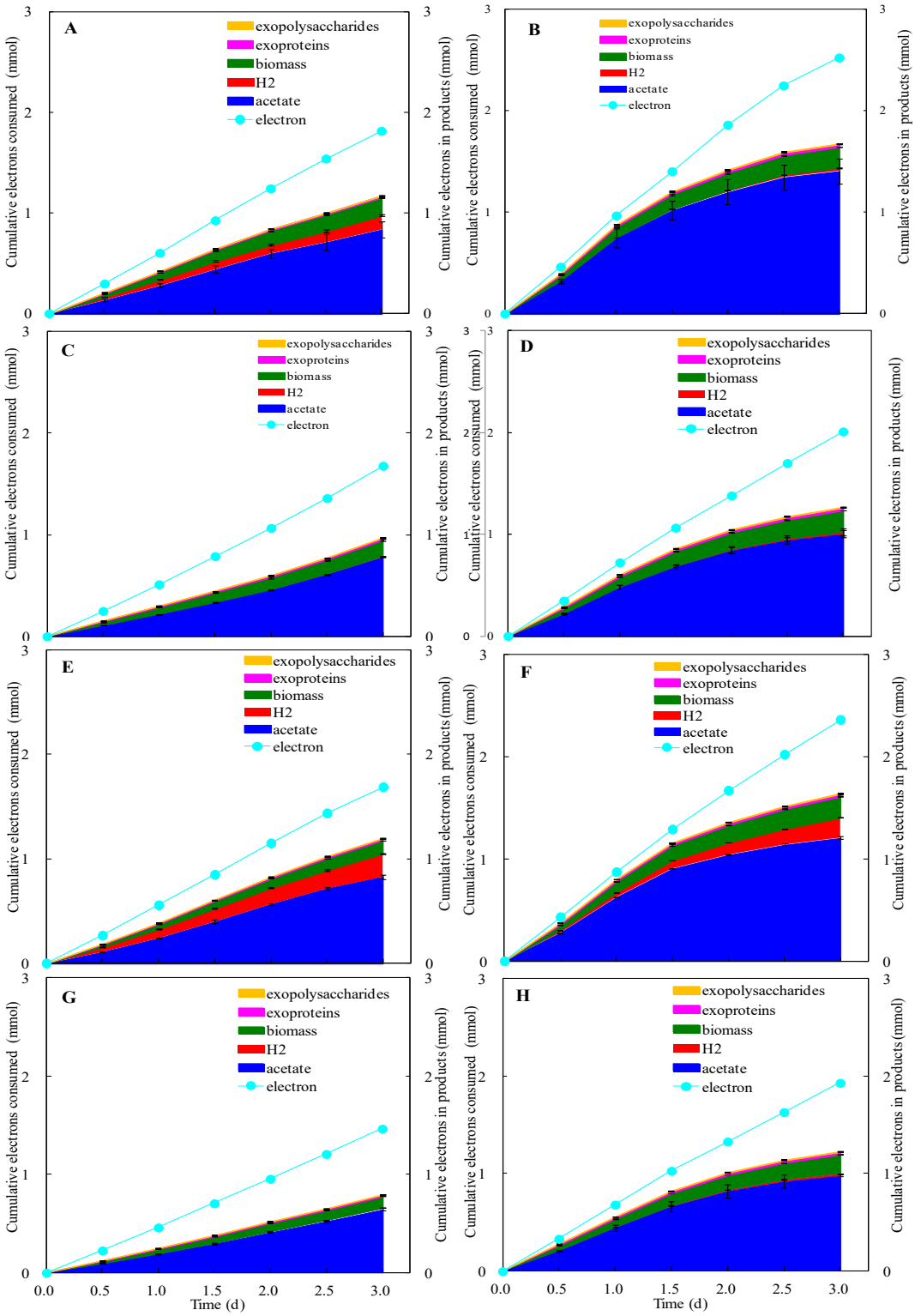

Figure 6 Time course of cumulative electrons either consumed or calculated in products in the *S. marcescens* Q1 (A – D) or the *Stenotrophomonas* sp. JY6 (E – H) catalyzed cathodes in the presence of both DNP and photo-irradiation (A and E), single photo-irradiation (B and F), or only DNP (C and G), or in the absence of both (D and H).

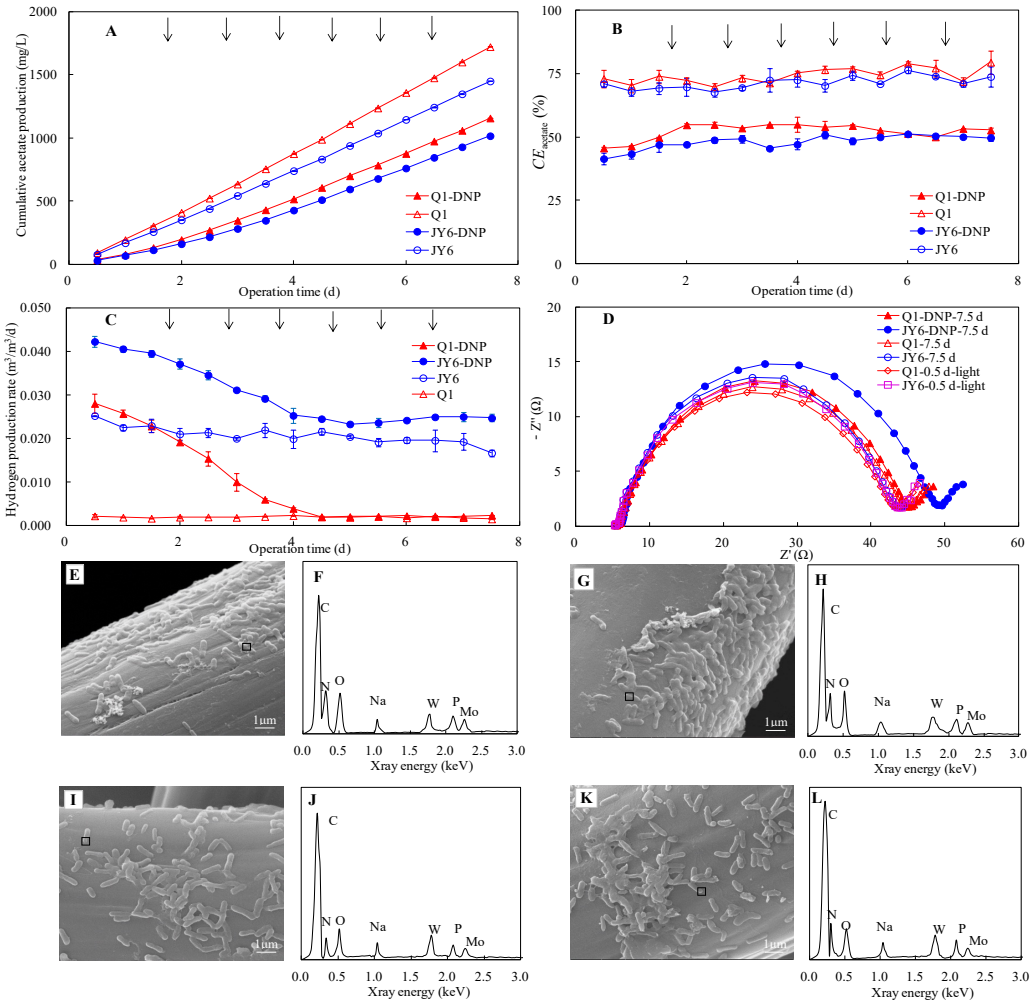

Figure 7 Time course of acetate production (A), coulombic efficiency for acetate production (B), hydrogen evolution (C) and impedance (D) in the *S. marcescens* Q1 or *Stenotrophomonas* sp. JY6 catalyzed cathodes in the presence or absence of DNP under same photo-irradiation. SEM observation (E, G, I and K) and EDS spectra (F, H, J and L) of either *S. marcescens* Q1 (E – H) or *Stenotrophomonas* sp. JY6 (I – L) catalyzed cathodes in the presence (E and I) or in the absence (G and K) of DNP at the end of 7.5 d operation.

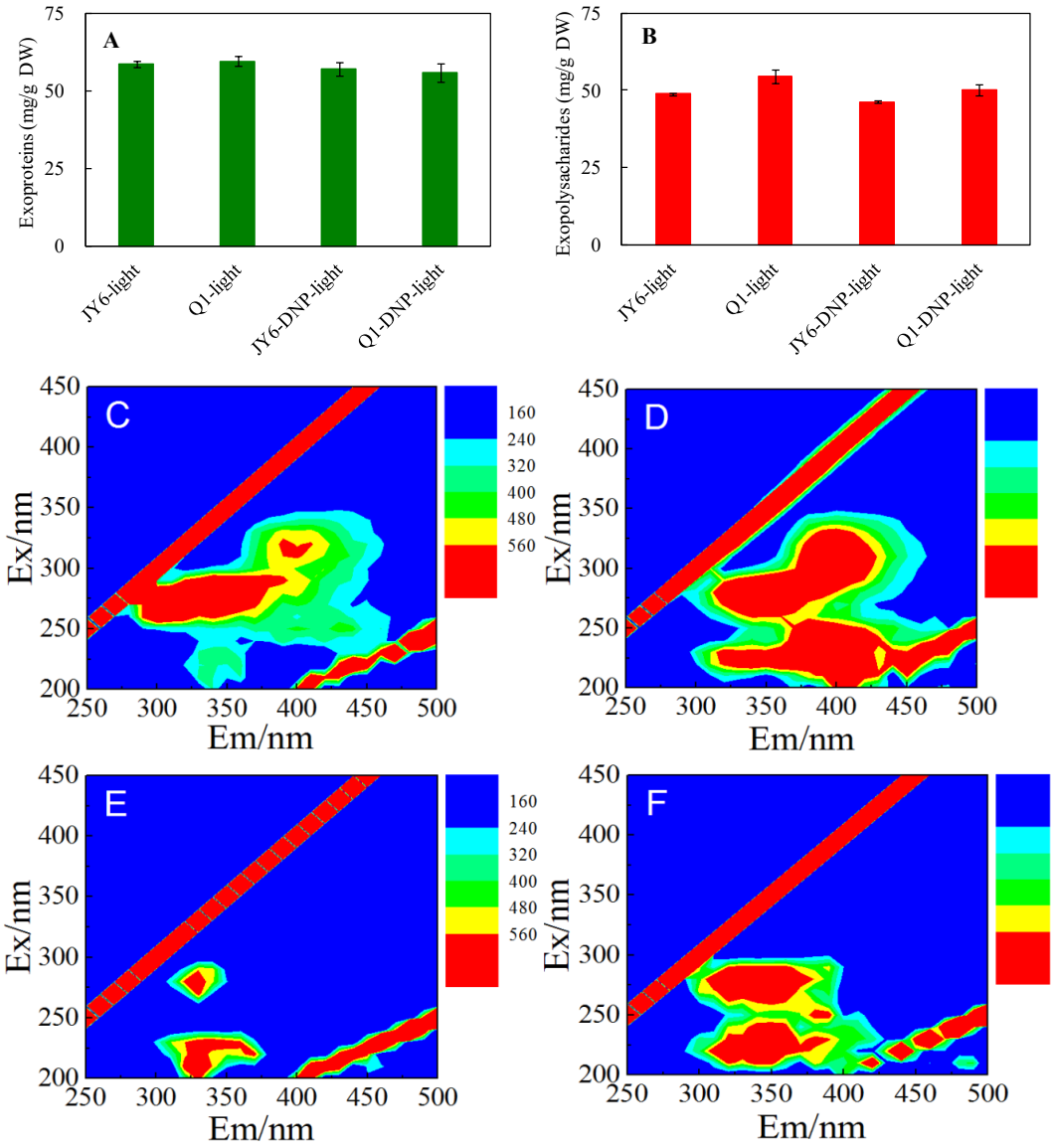

Figure 8 Comparison of exoproteins (A), exopolysaccharides (B), and three-dimensional excitation-emission matrix (EEM) fluorescence spectroscopy of extracellular polymer substances (C – F) produced by either cathodic *S. marcescens* Q1 (C and D) or *Stenotrophomonas* sp. JY6 (E and F) biofilms in the presence (A, B, C and E) or absence (A, B, D and F) of DNP at the end of 7.5 d operation.

Table 1 Comparison of direct and indirect (via H_2) extracellular electron transfers for the *S. marcescens* Q1 or the *Stenotrophomonas* sp. JY6 based on residual H_2 in the headspace in the presence of DNP and photo-irradiation

	Q1-DNP-light	Q1-light	JY6-DNP-light	JY6-light	Q1-DNP	Q1	JY6-DNP	JY6
Indirect electron transfer (%)	35 ± 2	22 ± 1	29 ± 0	18 ± 1	32 ± 5	14 ± 1	35 ± 1	15 ± 1
Acetate based indirect electron transfer (mg/L)	13 ± 0	21 ± 0	9 ± 0	14 ± 0	9 ± 1	9 ± 1	9 ± 1	9 ± 1
Direct electron transfer (%)	65 ± 2	78 ± 1	71 ± 0	82 ± 1	68 ± 5	86 ± 1	65 ± 1	85 ± 1
Acetate based direct electron transfer (mg/L)	25 ± 1	73 ± 6	22 ± 0	66 ± 1	20 ± 3	53 ± 1	18 ± 0	51 ± 0